*Met. Mater. Int., Vol. 15, No. 5 (2009), pp. 759~764*
doi: 10.1007/s12540-009-0759-8 Published 26 October 2009

# Characteristics of Plasma Electrolytic Oxide Coatings on Mg-Al-Zn Alloy Prepared by Powder Metallurgy

**Si Young Chang[1,*], Du Hyung Lee[2], Bo Sik Kim[3], Taek Soo Kim[4], Yo-Seung Song[1], Sung Ho Kim[5], and Chan Bok Lee[5]**

[1]Department of Materials Engineering, Korea Aerospace University, Gyeonggi 412-791, Korea
[2]Graduate student, Korea Aerospace University, Gyeonggi 412-791, Korea
[3]Undergraduate student, Korea Aerospace University, Gyeonggi 412-791, Korea
[4]Division for Advanced Materials, Korea Institute of Industrial Technology, Incheon 406-130, Korea
[5]Nuclear Materials Tech. Dev. Division, Korea Atomic Energy Research Institute, Daejeon 305-353, Korea

(received date: 1 April 2008 / accepted date: 1 April 2009)

Mg-6 wt.%Al-1 wt.%Zn alloy powders were produced by gas atomization, and subsequently compacted and sintered under various conditions of temperature, time, and pressure. The bulk Mg-6 wt.%Al-1 wt.%Zn alloy was coated by the plasma electrolytic oxidation (PEO) method. The optimum condition of compaction and sintering for PEO coatings was established based on the investigation of microstructure, microhardness, and corrosion properties of coatings which were compared to those of cast Mg-6 wt.%Al alloy. The coatings on Mg-6 wt.%Al and Mg-6 wt.%Al-1 wt.%Zn alloys consisted of MgO, $MgAl_2O_4$, and $Mg_2SiO_4$. The Mg-6 wt.%Al-1 wt.%Zn alloy compacted at room temperature for 10 min and sintered at 893 K for 3 h showed the most porous and nonuniform coating layer because the coatings had grown through grain boundaries that resulted from poor bonding between powder particles in the substrate. However, the coated Mg-6 wt.%Al-1 wt.%Zn alloy hot-compacted at 593 K for 10 min had the thickest coating layer and the highest microhardness. In addition, it demonstrated the best corrosion resistance as verified by polarization curves in 3.5% NaCl solution.

**Keywords:** gas atomization, Mg-Al-Zn alloy, sintering, plasma electrolytic oxidation mechanical and corrosion properties.

## 1. INTRODUCTION

Magnesium alloys are expected to be lightweight and highly efficient materials that can overcome the problems of environmental pollution and energy in all industrial fields because they have excellent dent resistance, damping capacity, and electromagnetic shielding capacity compared to plastics and aluminum alloys [1-4]. Therefore, they are becoming attractive, especially for the components of automobile and electronics. However, further applications of Mg alloys, generally produced by casting, have been limited due to their low hardness and poor corrosion and wear resistance. Applications can be expanded if these drawbacks can be overcome by surface treatment. Among powder metallurgy methods that produce near net shaped and complicated components in a simple process, gas atomization, due to rapid solidification, easily and safely allows microstructural modifications such as grain refinement, reduced segregation, and increased solubility [5]. In addition, the plasma electrolytic oxidation (PEO) treatment, which is an advancement of the conventional electrochemical anodizing treatment and leads to the local formation of a plasma by a spark on the metal surface, is expected to be a promising surface treatment [6]. Accordingly, the application of PEO treatment for gas-atomized Mg alloys is of interest to improve the mechanical and corrosion properties of Mg alloys. The goal in the present study is to investigate the characteristics, such as microstructure, microhardness, friction coefficient, and corrosion property, of PEO coatings on gas-atomized Mg-6 wt.%Al-1 wt.%Zn alloys by compaction and sintering under various conditions.

*Corresponding author: sychang@kau.ac.kr

## 2. EXPERIMENTAL PROCEDURE

The Mg-6 wt.%Al-1 wt.%Zn alloy powders were prepared by high pressure gas atomization. The details of the gas atomization procedure have been given in a recent report [7]. Figure 1 shows representative powders and powder particle distribution obtained by this method. The Mg-6 wt.%Al-1 wt.%Zn alloy powders have a near spherical morphology with a smooth surface and are between approximately 2 μm and 100 μm in diameter. The mean diameter of gas-atomized powders used in this study is 37 μm.

The powders were compacted and sintered under various conditions, designated as samples 2~4 and listed in Table 1. The cast Mg-6 wt.%Al alloy, designated as sample 1, was used as a comparison. The sintered samples were 11.4 mm in diameter and polished to approximately 0.2 μm in surface roughness prior to PEO coating. The Mg alloys and STS316L stainless steel were used as the anode and the cathode, respectively. AC power was applied with a 60 Hz modulation, applying both a positive and negative potential pulse for 1 s (C1 = 0.9 A), followed by a negative pulse for 0.2 s (C2 = 0.73 A) to the substrates immersed in electrolytes consisting of 5 *g*/*l* KOH and 8 *g*/*l* water glass ($2Na_2{\cdot}2SiO_3{\cdot}H_2O$). Power was controlled to maintain a constant current density of 20 $A/dm^2$ and coatings times were varied from 0 min to 50 min. Surface morphology and the cross section of coatings were observed with a scanning electron microscope (SEM) and the phases present in the coatings were analyzed by X-ray diffraction (XRD). Thickness and surface roughness were measured using an image analyzer and a SE-1700α surface roughness meter, respectively. Microhardness and the coefficient of friction of coatings were measured with a Vickers microhardness tester under a load of 50 g and a micro-scratch tester under a load of 20 N and speed of 0.5 mm/min, respectively. The corrosion resistance was evaluated by potentiodynamic polarization curves obtained from electrochemical tests in a 3.5% NaCl solution.

## 3. RESULTS AND DISCUSSION

Figure 2 shows microstructures of the starting Mg-6 wt.%Al and Mg-6 wt.%Al-1 wt.%Zn alloys before PEO treatment. The microstructure of sample 2 shows porosity between smaller grains, which results in small grains despite the higher sintering temperature, while samples 1, 3, and 4 exhibit no porosity at grain boundaries. Sample 4 has a larger grain size than sample 3, which results from grain growth during sintering in the case of sample 4. In the case of cast Mg-6 wt.%Al alloy (sample 1), the eutectic compound β-$Mg_{17}Al_{12}$ is homogeneously distributed in the Mg matrix from the homogenizing treatment [8,9], and the microstructure reveals the largest grain size compared to the gas-atomized Mg-6 wt.%Al-1 wt.%Zn alloy after compaction and sintering (samples 2~4).

Typical surface morphologies of coatings are shown in Fig. 3. All coatings have a porous surface microstructure with some volcano top-like pores randomly distributed and cracks in the area between the pores, which morphology is compatible with recently reported results [9-13]. However, there are differences in the size, shape and distribution of pores according to compaction and sintering conditions. Sample 1, the cast Mg-6 wt.%Al alloy, has the largest grain size and has relatively large pores and cracks, but the number

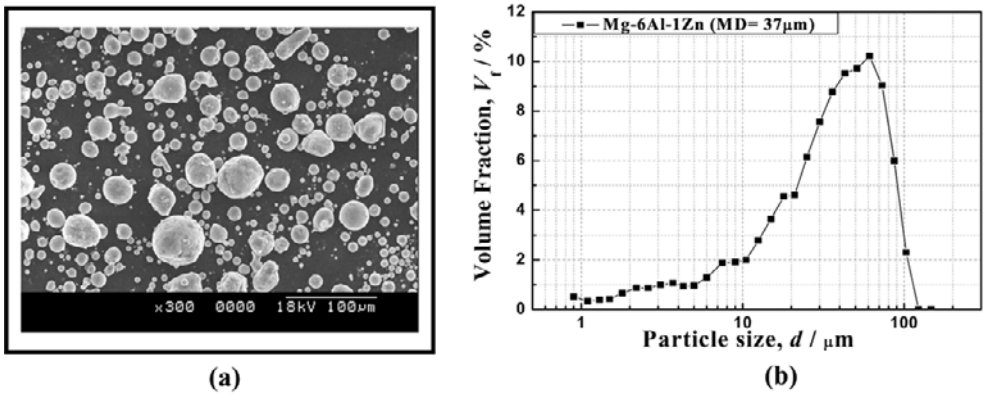


**Fig. 1.** SEM micrograph of the Mg-6 wt.%Al-1 wt.%Zn powders prepared by gas atomization (a) and powder particles distribution (b).

**Table 1.** Compaction and sintering conditions employed in this study

| | Sample | Compaction | Sintering |
|---|---|---|---|
| 1 | Mg-6 wt.%Al (cast) | - | 16 h at 693 K (Homogeneous treatment) |
| 2 | Mg-6 wt.%Al-1 wt.%Zn (powder) | 700 MPa for 10 min at R.T. | 3 h at 893 K |
| 3 | Mg-6 wt.%Al-1 wt.%Zn (powder) | 700 MPa for 10 min at 593 K | - |
| 4 | Mg-6 wt.%Al-1 wt.%Zn (powder) | 700 MPa for 10 min at 593 K | 24 h at 693 K |

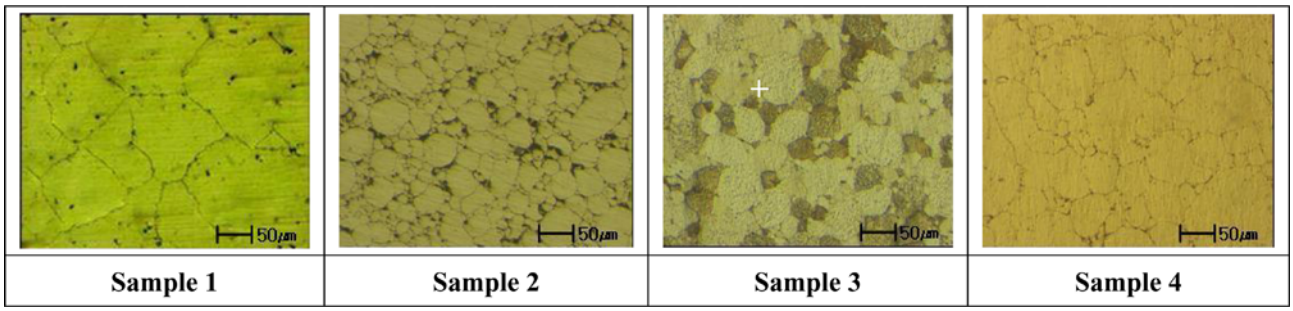


**Fig. 2.** Microstructures of Mg-6 wt.%Al and Mg-6 wt.%Al-1 wt.%Zn alloys.

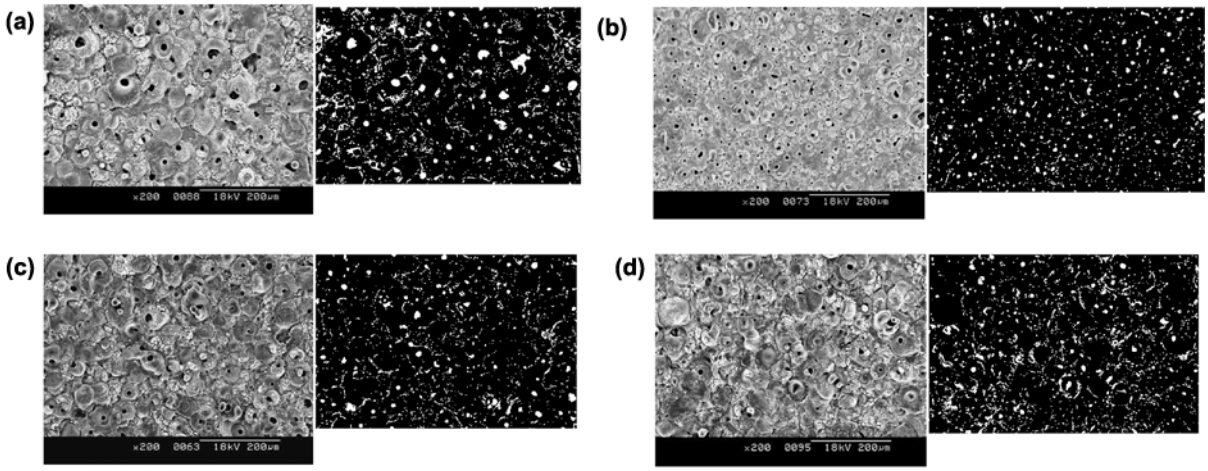


| Sample | Porosity (%) |
|---|---|
| 1 | 12.6 |
| 2 | 10.4 |
| 3 | 8.7 |
| 4 | 11.9 |

**Fig. 3.** Surface morphologies of PEO coatings and porosity fraction: (a) sample 1, (b) sample 2, (c) sample 3 and (d) sample 4.

of pores appears to be lower than that of other samples. For samples 2~4, which have small grains compared to sample 1, the pores and cracks on the surface are smaller. In particular, sample 2, with the smallest grain size and high porosity at the grain boundaries, has many small pores relatively well distributed on the surface. These results indicate that the formation of pores and cracks on the surface of coatings has a close relation to the microstructure of the substrate. Additionally, the volume fraction of the surface occupied by the pores and cracks was quantified by image analysis software. Sample 1 has the highest volume fraction of pores compared to samples 2~4, which were compacted and sintered. Among samples 2~4, sample 3, compacted by 700 MPa for 10 min at 593 K, has the lowest volume fraction of pores and cracks.

Figure 4 shows typical cross-sections of the PEO coatings on Mg-6 wt.%Al-1 wt.%Zn alloys. Increasing the coating time increases the thickness of the coated layer, which was characterized by a dense and porous structure. The porous microstructure near the surface is common in the PEO coatings [6,10]. The surface and interface between the oxide layer and the substrate are non-uniform, resulting in non-uniform coating thickness. The coating on sample 2 was the most porous and non-uniform. The coating layer grew through grain boundaries in the substrate with increasing coating time, most likely because of the presence of intergranular porosity in the substrate.

Figure 5 shows the XRD patterns for coatings grown for 50 min on cast Mg-6 wt.%Al (sample 1) and hot-compacted Mg-6 wt.%Al-1 wt.%Zn (sample 3) alloys. It is seen that the

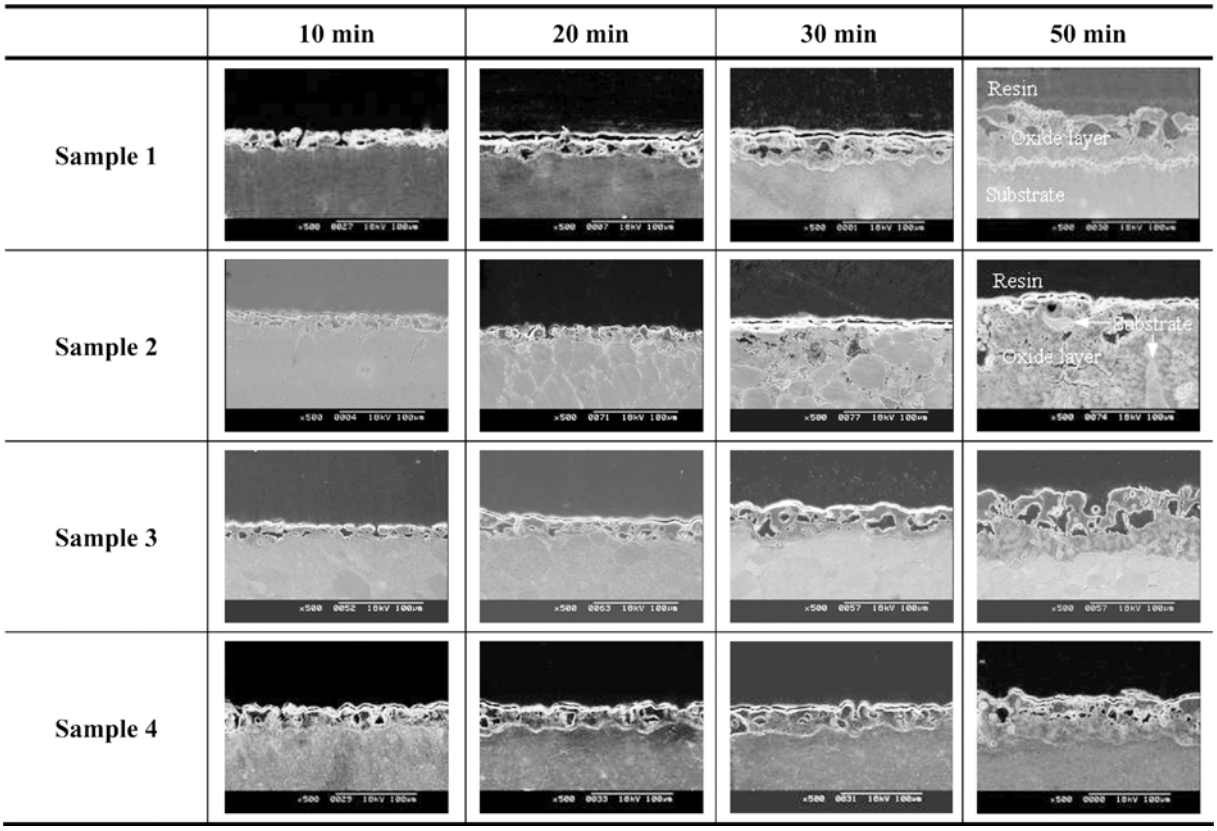


**Fig. 4.** Typical microstructures showing the cross-section of PEO coatings on Mg-6 wt.%Al and Mg-6 wt.%Al-1 wt.%Zn alloys with increasing coating time.

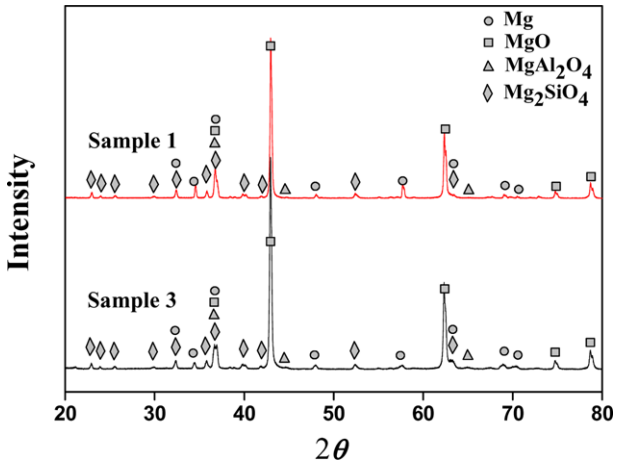


**Fig. 5.** XRD patterns of PEO coatings on Mg-6 wt.%Al and Mg-6 wt.%Al-1 wt.%Zn alloys coated for 50 min.

coatings contain MgO, $MgAl_2O_4$ and $Mg_2SiO_4$ in both of the samples. The formation of $MgAl_2O_4$ is consistent with recent results on AM60B Mg alloy coated by the PEO method [6]. It is reasonably well known that the formation of $Mg_2SiO_4$ is contributed to by Si decomposed from the water glass used in this study, as reported in a work on PEO coated AZ31B Mg alloy [14]. There is no difference in the phases present in the PEO coatings for all of the samples.

The surface roughness and thickness of the coatings are plotted in Fig. 6. The surface roughness increases gradually with increasing coating time except for sample 2, for which surface roughness increases until 20 min and then decreases. The thickness also increases as the coating time increases. All samples have a coating thickness of approximately 60 μm after coating for 50 min. However, the coatings of sample 2 are markedly thicker than those of the other samples because of rapid, discontinuous growth of the coatings through the grain boundary as shown in Fig. 4.

Figure 7 shows the microhardness of the PEO coatings, together with that of the uncoated substrates. In this study, the microhardness was measured from a dense layer in the cross-section shown in Fig. 4. The uncoated samples have a hardness of approximately 70 Hv. After coating, however, the microhardness of the coatings is much higher than that of the uncoated samples, and it increases with increasing coating time. In particular, the samples coated for 50 min, except for sample 2, which shows a porous coating layer, have a hardness of approximately 500 Hv in the dense layer region, which is superb compared to the conventional anodic oxide coatings on AZ91 magnesium alloy [15]. Among these

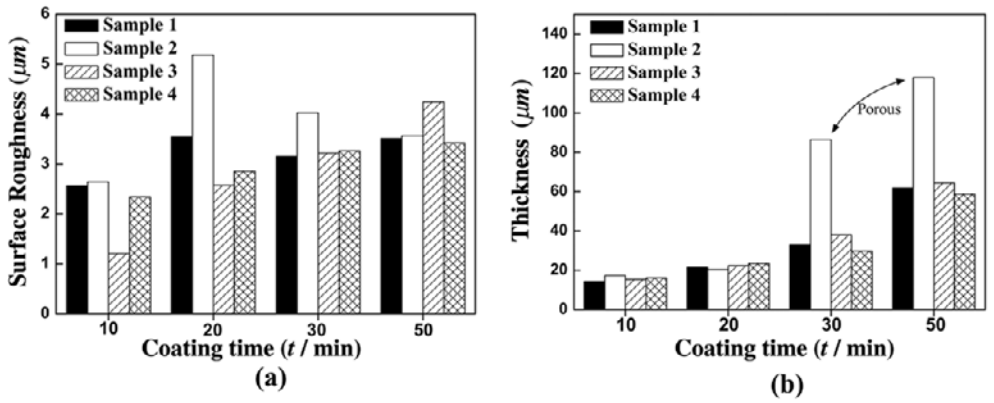


**Fig. 6.** Surface roughness (a) and thickness (b) of coatings on Mg-6 wt.%Al and Mg-6 wt.%Al-1 wt.%Zn alloys with increasing coating time.

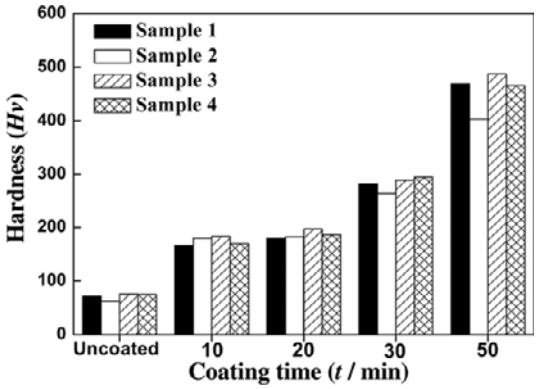


**Fig. 7.** Microhardness of coatings on Mg-6 wt.%Al and Mg-6 wt.%Al-1 wt.%Zn alloys with increasing coating time.

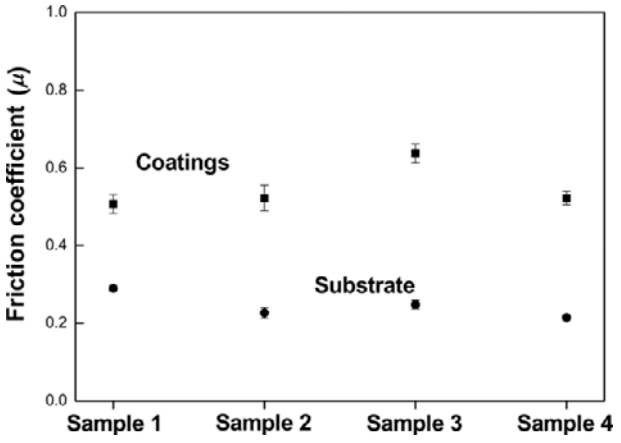


**Fig. 8.** Friction coefficient of coatings on Mg-6 wt.%Al and Mg-6 wt.%Al-1 wt.%Zn alloys after coating for 50 min.

samples, sample 3 exhibits the highest hardness after coating for 50 min.

Figure 8 shows the friction coefficients of coatings on samples after coating for 50 min, along with the friction coefficient for the Mg substrate. Before coating, sample 1 has a slightly higher friction coefficient compared to samples 2~4. However, all coatings on samples 1~4 exhibit higher friction coefficients than that of the Mg substrates. The coatings on sample 3 have the highest friction coefficient, in particular, while the other samples have nearly the same friction coefficient. The values of friction coefficient correspond to the results of surface roughness, thickness and microhardness for all coatings except those on sample 2. It is reasonably well understood why the coatings on sample 2, with its thick porous layer and low microhardness, show friction coefficients similar to those on samples 1 and 4. The reason is that the friction coefficient as measured by the micros-cratch test used in this study reflect the bonding of oxides without relation to the micro-porous structure shown in Fig. 4, unlike microhardness, which includes the effect of porous structure.

The corrosion properties of the coatings in a 3.5% NaCl solution for samples coated for 50 min are shown in Fig. 9. Samples 2~4, produced by powder metallurgy, have higher rest potentials and lower corrosion rates than sample 1 does. In particular, the hot-compacted Mg-6 wt.%Al-1 wt.%Zn alloy (sample 3) demonstrated the best corrosion resistance. This could be understood by the fact that the corrosion resistance corresponds to the measured volume fraction of pores and cracks on the surface, as represented in Fig. 3, because the pores and cracks could act as a path for penetration of the corrosion solution. In other words, the coatings on sample 3, which sample has the lowest volume fraction of pores and cracks, are strongest against corrosion, while the coating on sample 1 shows the worst corrosion resistance due to the many large pores and cracks on the surface of the coating despite the fact that it has a hardness and friction coefficient that is comparable to those of samples 2 and 4. Consequently, it is suggested from the above results that better corrosion resistance can be obtained in the coatings on Mg alloys produced by powder metallurgy than can be obtained by casting. Based on the results of microstructual characteristics, microhardness, and corrosion properties, it is apparent that the relatively homogeneous microstructure

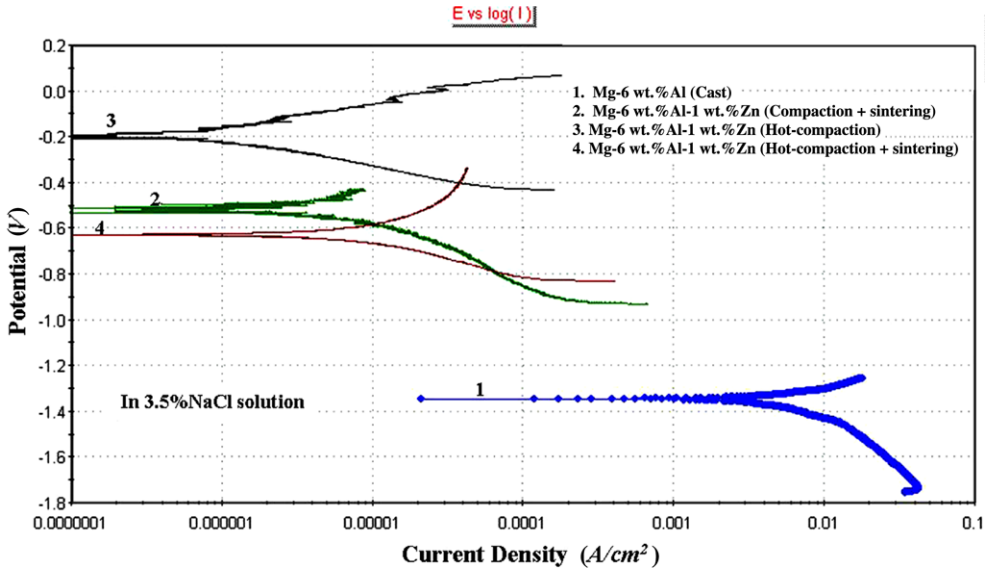


**Fig. 9.** Polarization curves in a 3.5% NaCl solution for Mg-6 wt.%Al and Mg-6 wt.%Al-1 wt.%Zn alloys coated for 50 min.

attained by only hot compaction is effective for obtaining coatings by the PEO method.

## 4. CONCLUSIONS

The coatings on gas-atomized Mg-6 wt.%Al-1 wt.%Zn alloy consisted of MgO, $MgAl_2O_4$, and $Mg_2SiO_4$, which were independent of compaction and sintering conditions. The surface roughness and thickness increased gradually with increasing coating time except for the gas-atomized Mg-6 wt.%Al-1 wt.%Zn alloy compacted by 700 MPa for 10 min at room temperature and sintered at 893 K for 3 h. The coatings on gas-atomized Mg-6 wt.%Al-1 wt.%Zn alloy showed an increase of microhardness as the coating time increased. In particular, the coatings on gas-atomized Mg-6 wt.%Al-1 wt.%Zn alloy only hot-compacted under 700 MPa for 10 min at 593 K exhibited the highest thickness and microhardness and rest potential in a 3.5% NaCl solution. In addition, the Mg-6 wt.%Al-1 wt.%Zn alloy prepared by powder metallurgy revealed better characteristics of PEO coatings than those of the cast Mg-6 wt.%Al alloy.

## ACKNOWLEDGMENTS

This work has been carried out as a part of the development of basic key technologies for Gen IV SFR fuel under the mid- and long-term nuclear R&D plans by the Korean Ministry of Science and Technology.

## REFERENCES

1. Y. Kojima and S. Kamado, *Mater. Sci. Forum* **488**, 9 (2005).
2. B. H. Choi, B. S. You, and I. M. Park, *Met. Mater. Int.* **12**, 63 (2006).
3. N. J. Park, J. H. Hwang, and J. S. Roh, *J. Kor. Inst. Met. & Mater.* **47**, 1 (2009).
4. B. S. Shin, Y. Kim, and D. H. Bae, *J. Kor. Inst. Met. & Mater.* **46**, 1 (2008).
5. M. Sugamata, S. Hanawa, and J. Kaneko, *Mater. Sci. Eng. A* **226-228**, 861 (1997).
6. A. L. Yerokhin, X. Nie, A. Leyland, A. Matthews, and S. J. Dowey, *Surf. Coat. Tech.* **122**, 73 (1999).
7. Y. Kawamura, K. Hayashi, A. Inoue, and T. Matsumoto, *Mater. Trans.* **42**, 1172 (2001).
8. D. J. Sakkinen, *SAE Technical Paper Series*, 940779.
9. Japan Inst. of Magnesium, *Handbook of Advanced Magnesium Technology*, p. 144, Kallos Publishing Co., Tokyo (2000).
10. J. Liang, B. Guo, J. Tian, H. Liu, J. Zhou, and T. Xu, *Appl. Surf. Sci.* **252**, 345 (2005).
11. J. A. Curran and T. W. Clyne, *Surf. Coat. Tech*. **199**, 177 (2005).
12. B. H. Song, Y. L. Kim, and S. Y. Chang, *Sol. St. Phen.* **124-126**, 763 (2007).
13. S. Y. Chang, Y. L. Kim, B. H. Song, and J. H. Lee, *Mater. Sci. Forum* **539-543**, 1224 (2007).
14. H. Guo, M. An, S. Xu, and H. Huo, *Mater. Lett.* **60**, 1538 (2006).
15. Japan Inst. of Magnesium, *Handbook of Advanced Magnesium Technology*, p. 343-345, Kallos Publishing Co., Tokyo (2000).